Conference Proceedings of the Society for Experimental Mechanics Series

Matt Allen · Randy Mayes · Daniel Rixen *Editors*

Dynamics of Coupled Structures, Volume 1

Proceedings of the 32nd IMAC, A Conference and Exposition on Structural Dynamics, 2014

SEM

Springer

Matt Allen • Randy Mayes • Daniel Rixen
Editors

Dynamics of Coupled Structures, Volume 1

Proceedings of the 32nd IMAC, A Conference and Exposition on Structural Dynamics, 2014

Springer

Editors
Matt Allen
Engineering Physics Department
University of Wisconsin Madison
Madison, WI, USA

Daniel Rixen
Lehrstuhl fur Angewandte Mechanik
Technische Universitat Munchen
Garching, Germany

Randy Mayes
Sandia National Laboratories
Albuquerque, NM, USA

ISSN 2191-5644 ISSN 2191-5652 (electronic)
ISBN 978-3-319-04500-9 ISBN 978-3-319-04501-6 (eBook)
DOI 10.1007/978-3-319-04501-6
Springer Cham Heidelberg New York Dordrecht London

Library of Congress Control Number: 2014932412

Preface

Dynamics of Coupled Structures, Volume 1 represents one of the eight volumes of technical papers presented at the 32nd IMAC, A Conference and Exposition on Structural Dynamics, 2014, organized by the Society for Experimental Mechanics, and held in Orlando, Florida, February 3–6, 2014. The full proceedings also include volumes on Nonlinear Dynamics; Model Validation and Uncertainty Quantification; Dynamics of Civil Structures; Structural Health Monitoring; Special Topics in Structural Dynamics; Topics in Modal Analysis I; and Topics in Modal Analysis II.

Each collection presents early findings from experimental and computational investigations on an important area within structural dynamics. Coupled structures, or substructuring, is one of these areas.

Substructuring is a general paradigm in engineering dynamics where a complicated system is analyzed by considering the dynamic interactions between subcomponents. In numerical simulations, substructuring allows one to reduce the complexity of parts of the system in order to construct a computationally efficient model of the assembled system. A subcomponent model can also be derived experimentally, allowing one to predict the dynamic behavior of an assembly by combining experimentally and/or analytically derived models. This can be advantageous for subcomponents that are expensive or difficult to model analytically. Substructuring can also be used to couple numerical simulation with real-time testing of components. Such approaches are known as hardware-in-the-loop or hybrid testing.

Whether experimental or numerical, all substructuring approaches have a common basis, namely the equilibrium of the substructures under the action of the applied and interface forces and the compatibility of displacements at the interfaces of the subcomponents. Experimental substructuring requires special care in the way the measurements are obtained and processed in order to assure that measurement inaccuracies and noise do not invalidate the results. In numerical approaches, the fundamental quest is the efficient computation of reduced order models describing the substructure's dynamic motion. For hardware-in-the-loop applications difficulties include the fast computation of the numerical components and the proper sensing and actuation of the hardware component. Recent advances in experimental techniques, sensor/actuator technologies, novel numerical methods, and parallel computing have rekindled interest in substructuring in recent years leading to new insights and improved experimental and analytical techniques.

The organizers would like to thank the authors, presenters, session organizers, and session chairs for their participation in this track.

Madison, WI, USA — M. Allen
Albuquerque, NM, USA — R. Mayes
Garching, Germany — D. Rixen

Contents

Chapter 1
Experimental-Analytical Dynamic Substructuring of Ampair Testbed: A State-Space Approach

Mladen Gibanica, Anders T. Johansson, Anders Liljerehn, Per Sjövall, and Thomas Abrahamsson

Abstract The Society for Experimental Mechanics (SEM) Substructuring Focus Group has initiated a research project in experimental dynamic substructuring using the Ampair 600W wind turbine as a testbed. In this paper, experimental as well as analytical models of the blades of said wind turbine are coupled to analytical models of its brackets. The focus is on a state-space based substructuring method designed specifically for experimental-analytical dynamic substructuring. It is shown (a) theoretically that the state-space method gives equivalent results to the second order methods under certain conditions, (b) that the state-space method numerically produces results equivalent to those of a well-known frequency-based substructuring technique when the same experimental models are used for the two methods and (c) that the state-space synthesis procedure can be translated to the general framework given by De Klerk et al.

Keywords Substructuring • Experimental-analytical dynamic • Modal analysis • Vibration testing • State-space • Component mode synthesis • Frequency based substructuring • Automatic system identification • Wind turbines

1.1 Introduction

The subject of substructuring has been an open research area ever since its advent in the 1960s [1]. Recently, often attributed to advances in computing capacity and experimental equipment, there has been a renewed interest in the subject. Substructuring builds on the idea that a complex structure can be decomposed into a number of simpler components, or substructures. The modeling approach of these substructures may vary, which allows creating mixed experimental and analytical models thereby increasing the modeling flexibility for complex mechanical structures such as cars, air planes, rocket launchers and wind turbines.

Although the main concept of substructuring is simple—a matter of enforcing compatibility and equilibrium at the interfaces between substructures—there are a number of different methods presented in literature. These are typically categorized, by the type of substructure models used, as Frequency Response Function (FRF) based and modal based (CMS—component mode synthesis) methods. Early works falling in the former category are e.g. [2, 3] while the Craig-Bampton method [4] is a well-known early representative of the latter. The paper by de Klerk et al. [1] is frequently cited as a well written overview of the field. This paper is based on the MSc thesis by Mr. Mladen Gibanica [5].

The structure under investigation here is the SEM Substructuring Focus Group testbed, the Ampair 600 wind turbine, further detailed by Mayes [6]. Since its introduction at IMAC XXX, several attempts at substructuring have been reported for this structure. A group from Sandia National Laboratories have worked with experimental substructuring using the Transmission Simulator Technique [7, 8], a method also employed at the Atomic Weapons Establishment in the UK [9],

M. Gibanica • A.T. Johansson (✉) • T. Abrahamsson
Department of Applied Mechanics, Chalmers University of Technology, SE-412 96 Göteborg, Sweden
e-mail: anders.t.johansson@chalmers.se

A. Liljerehn
AB Sandvik Coromant, R & D Metal Cutting Research, SE-811 81 Sandviken, Sweden

P. Sjövall
FS Dynamics, SE-412 63 Göteborg, Sweden

M. Allen et al. (eds.), *Dynamics of Coupled Structures, Volume 1: Proceedings of the 32nd IMAC, A Conference and Exposition on Structural Dynamics, 2014*, Conference Proceedings of the Society for Experimental Mechanics Series,
DOI 10.1007/978-3-319-04501-6_1, © The Society for Experimental Mechanics, Inc. 2014

while a frequency-based method was used by a group from TU Delft [10]. Also, a group of Italian scientists have studied the role of interface degrees of freedom for the coupling of the structure [11].

The purpose of the test bed is to serve as a reference for researchers around the world. Data is shared online through a wiki [12]. This paper considers the blades and the brackets of the turbine only—the hub, tower and base are thus left for later studies. The dynamics of the joints has not been considered (a presentation on nonlinear effects from varying contact geometry at different load levels was given by Dr. Pascal Reuss at IMAC XXXI [13]). Components are coupled using the state-space synthesis method of [14]. (Similar methods have been proposed also by e.g. Su and Juang [15].) The results are compared to experimental measurements of the assembly as well as experimental-analytical FRF-based coupling techniques and analytical models coupled using CMS. The Ampair 600 wind turbine blades, consisting of a composite hull around a solid core, have been thoroughly tested in dynamic and static measurements as well as destructive tests to quantify the material parameters [16–21]. A calibrated FE model of the blades has been developed by Johansson et al. [20] which is used for comparison here. A new FE model of the bracket is created from geometry measurements made available by the TU Delft and using standard material properties.

The paper is structured as follows: Sect. 1.2 briefly introduces the theory behind the state space coupling technique and puts it into the framework of de Klerk et al. [1]. Section 1.3 describes the Finite Element models used. Section 1.4 elaborates on performed experiments and describes the experimentally derived models used. Section 1.5 relates results before the paper is rounded up by some conclusions in Sect. 1.6.

1.2 Theory

In linear system theory, systems are sometimes separated into *external* and *internal* descriptions, where the former offer information on the input-output relation only whereas the latter includes information on the *state* of the process [22, 23]. The typical external model in structural dynamics is the time domain convolution relation which gives rise to the Frequency Response Function in the frequency domain:

$$\mathbf{y}(t) = \mathbf{y}_0 + \int_0^\infty \mathbf{h}(t-\tau)\mathbf{u}(\tau)d\tau \tag{1.1}$$

$$\mathbf{Y}(\omega) = \mathbf{H}(\omega)\mathbf{U}(\omega) \tag{1.2}$$

While internal models are given in the usual first- or second-order forms [24]:

$$\begin{cases} \dot{\mathbf{x}}(t) = \mathbf{A}\mathbf{x}(t) + \mathbf{B}\mathbf{u}(t) \\ \mathbf{y}(t) = \mathbf{C}\mathbf{x}(t) + \mathbf{D}\mathbf{u}(t) \end{cases} \tag{1.3}$$

$$\mathbf{K}\mathbf{q}(t) + \mathbf{V}\dot{\mathbf{q}}(t) + \mathbf{M}\ddot{\mathbf{q}}(t) = \mathbf{f}(t) \tag{1.4}$$

where the matrices have the usual meanings and the forces in Eq. (1.4) relate to the input in Eq. (1.3) through a selection matrix such that $\mathbf{f}(t) = \mathbf{P}_u\mathbf{u}(t)$ [25]. A shaker or impact hammer testing campaign will thus result in an external model of the system, from which the analyst frequently attempts to derive an internal model. This process is often referred to as *modal parameter extraction* [26] in the structural dynamics community and *system identification* elsewhere [27].

1.2.1 System Identification

System identification is performed on experimentally obtained outer models in the frequency domain, Eq. (1.2), using the state-space subspace system identification algorithm implemented as `n4sid` in MATLAB's System Identification Toolbox [27, 28] to estimate a state-space model quadruple set $\{\mathbf{A}, \mathbf{B}, \mathbf{C}, \mathbf{D}\}$. In order to automate the system identification process a method for automatic model order estimation by Yaghoubi and Abrahamsson [29] is used along with the N4SID method.

All systems studied in this paper are considered to be linear time invariant (LTI) systems. By assumption they are also stable and passive. The systems are also assumed to be reciprocal (since the systems are non-gyroscopic and non-circulatory). As system identification is a general tool, these assumptions must be enforced explicitly (except for stability, which can be included as a condition on the system identification algorithm). Reciprocity is enforced through measuring using a limited

number of input nodes and applying Maxwell-Betti's reciprocity principle (see [5]). The passivity criterion states that the power supplied to the system is non-negative and can be zero only for components without damping. Models derived from first principles satisfy the passivity criterion implicitly, but this is not necessarily the case for experimentally identified models. The passivity problem for state space models is commonly known, for details see for example [14,30]. The passivity of a state space model is linked to the positive real (PR) lemma. In this paper, an engineering solution to the passivity optimization problem defined in [14] based on averaging of the **B** and **C** matrices has been used.

1.2.2 Substructuring

Substructuring is the process of coupling two structures together by enforcing two conditions at their common interface; compatibility and force equilibrium. This paper will treat only what de Klerk et al. [1] refers to as the primal formulation, which implies that the displacements are defined and interface forces are eliminated. For brevity, the explicit time dependency is dropped from the equations in the following.

For (analytically derived) internal models as in Eq. (1.4), enforcing compatibility and force equilibrium amounts to an assembly procedure parallel to that used for Finite Element Models, see further de Klerk et al. [1], such that synthesis of two systems 1 and 2 can be described by:

$$\begin{cases} \begin{bmatrix} \mathbf{K}_1 & \mathbf{0} \\ \mathbf{0} & \mathbf{K}_2 \end{bmatrix} \begin{Bmatrix} \mathbf{q}_1 \\ \mathbf{q}_2 \end{Bmatrix} + \begin{bmatrix} \mathbf{V}_1 & \mathbf{0} \\ \mathbf{0} & \mathbf{V}_2 \end{bmatrix} \begin{Bmatrix} \dot{\mathbf{q}}_1 \\ \dot{\mathbf{q}}_2 \end{Bmatrix} + \begin{bmatrix} \mathbf{M}_1 & \mathbf{0} \\ \mathbf{0} & \mathbf{M}_2 \end{bmatrix} \begin{Bmatrix} \ddot{\mathbf{q}}_1 \\ \ddot{\mathbf{q}}_2 \end{Bmatrix} = \mathbf{f} + \mathbf{g} \\ \mathbf{E}\mathbf{q} = \mathbf{0} \\ \mathbf{L}^T\mathbf{g} = \mathbf{0} \end{cases} \tag{1.5}$$

where **E** can be thought of as a signed boolean matrix enforcing compatibility,[1] **g** are the interface forces, and the matrix **L** is the nullspace of **E**. For details, refer to [1]. When coupling two structures, which are described by m_1 and m_2 degrees of freedom (DOFs), the assembled structure will consist of $m_1 + m_2 - m_c$ coordinates, where m_c is the number of coupling constraints. The de Klerk et al. paper [1] generalizes the formulation using the two matrices **E** and **L** to include also models using generalized coordinates and outer models (Eq. (1.2)), i.e. FRF coupling. In a following subsection, the state-space method [14] will be put into the same format.

1.2.3 State-Space Coupling

The state-space coupling used here is described in the paper by Sjövall and Abrahamsson [14]. At its core is the *coupling form* of Eq. (1.6), where the i:th first-order system to be coupled is rewritten to second-order form at the interface in order for the compatibility and force equilibrium conditions to be applicable

$$\begin{cases} \begin{bmatrix} \ddot{\mathbf{y}}_c \\ \dot{\mathbf{y}}_c \\ \dot{\mathbf{x}}_b \end{bmatrix} = \begin{bmatrix} \mathbf{A}^i_{vv} & \mathbf{A}^i_{vd} & \mathbf{A}^i_{vb} \\ \mathbf{I} & \mathbf{0} & \mathbf{0} \\ \mathbf{0} & \mathbf{A}^i_{bd} & \mathbf{A}^i_{bb} \end{bmatrix} \begin{bmatrix} \dot{\mathbf{y}}_c \\ \mathbf{y}_c \\ \mathbf{x}_b \end{bmatrix} + \begin{bmatrix} \mathbf{B}^i_{vv} & \mathbf{B}^i_{vb} \\ \mathbf{0} & \mathbf{0} \\ \mathbf{0} & \mathbf{B}^i_{bb} \end{bmatrix} \begin{bmatrix} \mathbf{u}_c \\ \mathbf{u}_d \end{bmatrix} \\ \begin{bmatrix} \mathbf{y}_c \\ \mathbf{y}_d \end{bmatrix} = \begin{bmatrix} \mathbf{0} & \mathbf{I} & \mathbf{0} \\ \mathbf{C}^i_{bv} & \mathbf{C}^i_{bd} & \mathbf{C}^i_{bb} \end{bmatrix} \end{cases} \tag{1.6}$$

Here, the subscript c refers to coupling degrees of freedom, b other degrees of freedom, v velocity outputs and d displacement outputs. Note that for state-space coupling there exist twice as many states as DOFs (a product of rewriting a second-order differential equation on first-order form) and thus if $n = 2m$, for two structures with n_1 and n_2 states and m_c coupling coordinates the coupled system will contain $n_1 + n_2 - 2m_c$ states.

[1] This matrix is denoted **B** in de Klerk et al. The notation cannot be adopted here as the **B** matrix is strongly associated to the state-space formulation in Eq. (1.3).

1.2.3.1 General Framework

Here, the coupling procedure derived in [14] is recast into the general framework established by de Klerk et al. [1], thus using the $\mathbf{E}$ and $\mathbf{L}$ matrices defined above.

Starting from a general state-space formulation (Eq. (1.3)), a transformation matrix $\mathbf{T}$ is introduced which takes the system to the coupling form of Eq. (1.6) [14]. Let the system on coupling form be:

$$\begin{cases} \dot{\tilde{\mathbf{x}}} = \tilde{\mathbf{A}}\tilde{\mathbf{x}} + \tilde{\mathbf{B}}\mathbf{u} \\ \mathbf{y} = \tilde{\mathbf{C}}\tilde{\mathbf{x}} \end{cases} \tag{1.7}$$

where $\tilde{\mathbf{A}} = \mathbf{T}^{-1}\mathbf{A}\mathbf{T}$, $\tilde{\mathbf{B}} = \mathbf{T}\mathbf{B}$, $\tilde{\mathbf{C}} = \mathbf{C}\mathbf{T}^{-1}$ and $\tilde{\mathbf{x}} = \mathbf{T}\mathbf{x}$. $\mathbf{B}_{vv}$ of Eq. (1.6) is the inertia at the interface DOFs [31]. By forming of a new matrix denoted $\mathbf{M}_B$, the system can be rewritten such that the first block row is pre-multiplied by $\mathbf{B}_{vv}^{-1}$. The matrix $\mathbf{M}_B$ will then be:

$$\mathbf{M}_B = diag(diag(\mathbf{B}_{vv}^{1^{-1}}, \mathbf{I}, \mathbf{I}), \ldots, diag(\mathbf{B}_{vv}^{h^{-1}}, \mathbf{I}, \mathbf{I})) \tag{1.8}$$

Such that the system can now be written as:

$$\begin{cases} \mathbf{M}_B\dot{\tilde{\mathbf{x}}} = \mathbf{M}_B\tilde{\mathbf{A}}\tilde{\mathbf{x}} + \mathbf{M}_B\tilde{\mathbf{B}}\mathbf{u} \\ \mathbf{y} = \tilde{\mathbf{C}}\tilde{\mathbf{x}} \end{cases} \tag{1.9}$$

Introducing the $\mathbf{E}$ and $\mathbf{L}$ matrices such that compatibility is described by $\mathbf{E}\tilde{\mathbf{x}} = \mathbf{0}$ and equilibrium by $\mathbf{L}^T\mathbf{u}_{c,g} = \mathbf{0}$, where subscript g is used to denote interface forces, the matrix $\mathbf{L}$ is formed as $\mathbf{L} = null(\mathbf{E})$ such that the following is satisfied: $\mathbf{E}\tilde{\mathbf{x}} = \mathbf{E}\mathbf{L}\tilde{\mathbf{z}} = \mathbf{0}$ and $\tilde{\mathbf{x}} = \mathbf{L}\tilde{\mathbf{z}}$. The new state vector $\tilde{\mathbf{z}}$ represents the new states after coupling. The synthesised state-space model is then formed as follows:

$$\begin{cases} \mathbf{L}^T\mathbf{M}_B\mathbf{L}\dot{\tilde{\mathbf{z}}} = \mathbf{L}^T\mathbf{M}_B\tilde{\mathbf{A}}\mathbf{L}\tilde{\mathbf{z}} + \mathbf{L}^T\mathbf{M}_B\tilde{\mathbf{B}}\mathbf{u} \\ \mathbf{y} = \tilde{\mathbf{C}}\mathbf{L}\tilde{\mathbf{z}} \end{cases} \tag{1.10}$$

Finally, $(\mathbf{L}^T\mathbf{M}_B\mathbf{L})^{-1}$, may be pre-multiplied to the first equation in Eq. (1.10). A new transformation matrix must however be introduced simply to reduce the excess inputs and outputs. The new matrix is denoted $\mathbf{L}_u$ and is formed from a matrix $\mathbf{E}_u$ as before, $\mathbf{L}_u = null(\mathbf{E}_u)$. In other words, for a system with two synthesised components the new reduction matrix is $\mathbf{E}_u = [\mathbf{I} \quad \mathbf{0} \quad \mathbf{0} \quad \mathbf{0}]$. The implication of this transformation is that in the synthesised model, to which this new matrix is applied, the first component of the considered vector will be removed. This new matrix is introduced in the equations by the transformations $\mathbf{u} = \mathbf{L}_u\bar{\mathbf{u}}$ and $\bar{\mathbf{y}} = \mathbf{L}_u^T\mathbf{y}$ as shown in Eq. (1.12). The last step is only true for systems with an equal number of inputs and outputs but is easily generalised. The final system can be written as follows:

$$\begin{cases} \dot{\hat{\mathbf{z}}} = \hat{\mathbf{A}}\hat{\mathbf{z}} + \hat{\mathbf{B}}\bar{\mathbf{u}} \\ \bar{\mathbf{y}} = \hat{\mathbf{C}}\hat{\mathbf{z}} \end{cases} \tag{1.11}$$

Where each part in the equation above is then identified as:

$$\begin{cases} \hat{\mathbf{A}} = (\mathbf{L}^T\mathbf{M}_B\mathbf{L})^{-1}(\mathbf{L}^T\mathbf{M}_B\tilde{\mathbf{A}}\mathbf{L}) \\ \hat{\mathbf{B}} = (\mathbf{L}^T\mathbf{M}_B\mathbf{L})^{-1}(\mathbf{L}^T\mathbf{M}_B\tilde{\mathbf{B}})\mathbf{L}_u \\ \hat{\mathbf{C}} = \mathbf{L}_u^T(\tilde{\mathbf{C}}\mathbf{L}) \end{cases} \tag{1.12}$$

1.2.3.2 Second Order Form Equivalent of Synthesised First Order Form

An analytical model written on second order form can easily be rewritten on first order form by doubling the number of states [24]. The transformation from a first order form to a second order form with half the number of states is not as trivial, even when possible.

Begin the second order system shown in Eq. (1.5). Methods for rewriting such a system to the first-order form of Eq. (1.3) are well-known [24, 25]. It is assumed that the output is the entire displacement vector, such that all DOFs are considered as

outputs. A transformation matrix is introduced in Eq. (1.13) which transforms a state-space system to coupling form under the assumption that the original system is analytically derived with state vector $\mathbf{x}^T = \begin{bmatrix}\mathbf{q}\ \dot{\mathbf{q}}\end{bmatrix}^T$ and displacement output such that $\mathbf{q} = \mathbf{y} = \mathbf{C}\mathbf{x}$

$$\mathbf{T}^i = \begin{bmatrix} \mathbf{C}_c^i \mathbf{A}^i \\ \mathbf{C}_c^i \\ \mathbf{C}_b^i \mathbf{A}^i \\ \mathbf{C}_b^i \end{bmatrix} \tag{1.13}$$

This transformation will produce a new state vector, $\tilde{\mathbf{x}} = \begin{bmatrix}\dot{\mathbf{y}}_c^i\ \mathbf{y}_c^i\ \dot{\mathbf{y}}_b^i\ \mathbf{y}_b\end{bmatrix}^T$, where the superscript i represents the subcomponent system. Again, the subscript c denotes the coupling partition of the input and output matrices, i.e. the block row and column of the **B** and **C** matrices, respectively. The difference between this transformation and the transformation in [14], is that the internal states are represented by physical coordinates here. In a theoretical representation this is valid, but in an experimental representation it would imply a significant constraint on the model to allow only twice as many states as there are sensors. The coupling form obtained through Eq. (1.13) is shown below

$$\begin{cases} \tilde{\mathbf{A}}^i = \mathbf{T}^i \mathbf{A}^i \mathbf{T}^{i^{-1}} = \begin{bmatrix} \mathbf{A}_{cvc}^i & \mathbf{A}_{cdc}^i & \mathbf{A}_{cvb}^i & \mathbf{A}_{cdb}^i \\ \mathbf{I} & \mathbf{0} & \mathbf{0} & \mathbf{0} \\ \mathbf{A}_{bvc}^i & \mathbf{A}_{bdc}^i & \mathbf{A}_{bvb}^i & \mathbf{A}_{bdb}^i \\ \mathbf{0} & \mathbf{0} & \mathbf{I} & \mathbf{0} \end{bmatrix} \\ \tilde{\mathbf{B}}^i = \mathbf{T}^i \mathbf{B}^i = \begin{bmatrix} \mathbf{C}_c^i \mathbf{A}^i \mathbf{B}^i \\ \mathbf{C}_c^i \mathbf{B}^i \\ \mathbf{C}_b^i \mathbf{A}^i \mathbf{B}^i \\ \mathbf{C}_b^i \mathbf{B}^i \end{bmatrix} = \begin{bmatrix} \mathbf{C}_c^i \mathbf{A}^i \mathbf{B}^i \\ \mathbf{0} \\ \mathbf{C}_b^i \mathbf{A}^i \mathbf{B}^i \\ \mathbf{0} \end{bmatrix} = \begin{bmatrix} \mathbf{B}_{c,c}^i & \mathbf{B}_{c,b}^i \\ \mathbf{0} & \mathbf{0} \\ \mathbf{B}_{bc}^i & \mathbf{B}_{bb}^i \\ \mathbf{0} & \mathbf{0} \end{bmatrix} \\ \tilde{\mathbf{C}}^i = \mathbf{C}^i \mathbf{T}^{i^{-1}} = \begin{bmatrix} \mathbf{I}\ \mathbf{0}\ \mathbf{0}\ \mathbf{0} \\ \mathbf{0}\ \mathbf{0}\ \mathbf{I}\ \mathbf{0} \end{bmatrix} \end{cases} \tag{1.14}$$

It can be shown that the transformation of the input matrix **CAB**, with the assumptions introduced above, is but the inverse of the mass matrix, thus simplifying the $\tilde{\mathbf{B}}$ matrix as follows (recall that the full system mass matrix is a block-diagonal matrix):

$$\begin{cases} \mathbf{B}_{cc}^i = \mathbf{M}_{cc}^{i^{-1}} \\ \mathbf{B}_{cb}^i = \mathbf{0} \\ \mathbf{B}_{bc}^i = \mathbf{0} \\ \mathbf{B}_{bb}^i = \mathbf{M}_{bb}^{i^{-1}} \end{cases} \tag{1.15}$$

Synthesising two systems by the procedure described above yields the following model, here reorganised such that it is recognisable as the usual state-space formulation of a second order system [25]:

$$\begin{Bmatrix} \dot{\bar{\mathbf{y}}}_c \\ \dot{\mathbf{y}}_b^1 \\ \dot{\mathbf{y}}_b^2 \\ \ddot{\bar{\mathbf{y}}}_c \\ \ddot{\mathbf{y}}_b^1 \\ \ddot{\mathbf{y}}_b^2 \end{Bmatrix} = \begin{bmatrix} \mathbf{0} & \mathbf{0} & \mathbf{0} & \mathbf{I} & \mathbf{0} & \mathbf{0} \\ \mathbf{0} & \mathbf{0} & \mathbf{0} & \mathbf{0} & \mathbf{I} & \mathbf{0} \\ \mathbf{0} & \mathbf{0} & \mathbf{0} & \mathbf{0} & \mathbf{0} & \mathbf{I} \\ \bar{\mathbf{A}}_{cdc} & \bar{\mathbf{A}}_{cdb}^1 & \bar{\mathbf{A}}_{cdb}^2 & \bar{\mathbf{A}}_{cvc} & \bar{\mathbf{A}}_{cvb}^1 & \bar{\mathbf{A}}_{cvb}^2 \\ \mathbf{A}_{bdc}^1 & \mathbf{A}_{bdb}^1 & \mathbf{0} & \mathbf{A}_{bvc}^1 & \mathbf{A}_{bvb}^1 & \mathbf{0} \\ \mathbf{A}_{bdc}^2 & \mathbf{0} & \mathbf{A}_{bdb}^2 & \mathbf{A}_{bvc}^2 & \mathbf{0} & \mathbf{A}_{bvb}^2 \end{bmatrix} \begin{Bmatrix} \bar{\mathbf{y}}_c \\ \mathbf{y}_b^1 \\ \mathbf{y}_b^2 \\ \dot{\bar{\mathbf{y}}}_c \\ \dot{\mathbf{y}}_b^1 \\ \dot{\mathbf{y}}_b^2 \end{Bmatrix} + \begin{bmatrix} \mathbf{0} & \mathbf{0} & \mathbf{0} \\ \mathbf{0} & \mathbf{0} & \mathbf{0} \\ \mathbf{0} & \mathbf{0} & \mathbf{0} \\ \bar{\mathbf{B}}_{cc} & \mathbf{0} & \mathbf{0} \\ \mathbf{0} & \mathbf{B}_{bb}^1 & \mathbf{0} \\ \mathbf{0} & \mathbf{0} & \mathbf{B}_{bb}^2 \end{bmatrix} \begin{Bmatrix} \bar{\mathbf{u}}_c \\ \mathbf{u}_b^1 \\ \mathbf{u}_b^2 \end{Bmatrix}$$

$$\begin{Bmatrix} \bar{\mathbf{y}}_c \\ \mathbf{y}_b^1 \\ \mathbf{y}_b^2 \end{Bmatrix} = \begin{bmatrix} \mathbf{I}\ \mathbf{0}\ \mathbf{0}\ \mathbf{0}\ \mathbf{0}\ \mathbf{0} \\ \mathbf{0}\ \mathbf{I}\ \mathbf{0}\ \mathbf{0}\ \mathbf{0}\ \mathbf{0} \\ \mathbf{0}\ \mathbf{0}\ \mathbf{I}\ \mathbf{0}\ \mathbf{0}\ \mathbf{0} \end{bmatrix} \begin{Bmatrix} \bar{\mathbf{y}}_c \\ \mathbf{y}_b^1 \\ \mathbf{y}_b^2 \\ \dot{\bar{\mathbf{y}}}_c \\ \dot{\mathbf{y}}_b^1 \\ \dot{\mathbf{y}}_b^2 \end{Bmatrix} \tag{1.16}$$

The lower part can be identified as a second order system which is directly comparable to the direct coupling procedure [1]. The two second order systems can be written with an interface part (c) and a body part (b) for two components, $i = 1, 2$.

$$\begin{cases} \mathbf{M}^i = \begin{bmatrix} \mathbf{M}^i_{cc} & \mathbf{0} \\ \mathbf{0} & \mathbf{M}^i_{bb} \end{bmatrix} \\ \mathbf{K}^i = \begin{bmatrix} \mathbf{K}^i_{cc} & \mathbf{K}^i_{cb} \\ \mathbf{K}^i_{bc} & \mathbf{K}^i_{bb} \end{bmatrix} \\ \mathbf{V}^i = \begin{bmatrix} \mathbf{V}^i_{cc} & \mathbf{V}^i_{cb} \\ \mathbf{V}^i_{bc} & \mathbf{V}^i_{cc} \end{bmatrix} \end{cases} \tag{1.17}$$

The synthesised system then becomes

$$\begin{cases} \mathbf{M}_{as} = \begin{bmatrix} \mathbf{M}^1_{cc} + \mathbf{M}^2_{cc} & \mathbf{0} & \mathbf{0} \\ \mathbf{0} & \mathbf{M}^1_{bb} & \mathbf{0} \\ \mathbf{0} & \mathbf{0} & \mathbf{M}^2_{bb} \end{bmatrix} \\ \mathbf{K}_{as} = \begin{bmatrix} \mathbf{K}^1_{cc} + \mathbf{K}^2_{cc} & \mathbf{K}^1_{cb} & \mathbf{K}^2_{cb} \\ \mathbf{K}^1_{bc} & \mathbf{K}^1_{bb} & \mathbf{0} \\ \mathbf{K}^2_{bc} & \mathbf{0} & \mathbf{K}^2_{bb} \end{bmatrix} \\ \mathbf{V}_{as} = \begin{bmatrix} \mathbf{V}^1_{cc} + \mathbf{V}^2_{cc} & \mathbf{V}^1_{cb} & \mathbf{V}^2_{cb} \\ \mathbf{V}^1_{bc} & \mathbf{V}^1_{bb} & \mathbf{0} \\ \mathbf{V}^2_{bc} & \mathbf{0} & \mathbf{V}^2_{bb} \end{bmatrix} \end{cases} \tag{1.18}$$

For comparison, the second order system from Eq. (1.16) is pre-multiplied by the inverse of its input matrix, which is diagonal. The resulting matrix is split in two, one part representing the stiffness and the other the damping. The following is then obtained

$$\begin{cases} \mathbf{M}_{as} \equiv \mathbf{M}_{sss} = \begin{bmatrix} \bar{\mathbf{B}}^{-1}_{cc} & \mathbf{0} & \mathbf{0} \\ \mathbf{0} & \bar{\mathbf{B}}^{1^{-1}}_{bb} & \mathbf{0} \\ \mathbf{0} & \mathbf{0} & \bar{\mathbf{B}}^{2^{-1}}_{bb} \end{bmatrix} = \begin{bmatrix} \mathbf{M}^1_{cc} + \mathbf{M}^2_{cc} & \mathbf{0} & \mathbf{0} \\ \mathbf{0} & \mathbf{M}^1_{bb} & \mathbf{0} \\ \mathbf{0} & \mathbf{0} & \mathbf{M}^2_{bb} \end{bmatrix} \\ \mathbf{K}_{as} \equiv \mathbf{K}_{sss} = \begin{bmatrix} \bar{\mathbf{B}}^{-1}_{cc}\bar{\mathbf{A}}_{cdc} & \bar{\mathbf{B}}^{-1}_{cc}\bar{\mathbf{A}}^1_{cdb} & \bar{\mathbf{B}}^{-1}_{cc}\bar{\mathbf{A}}^2_{cdb} \\ \bar{\mathbf{B}}^{1^{-1}}_{bb}\mathbf{A}^1_{bdc} & \bar{\mathbf{B}}^{1^{-1}}_{bb}\mathbf{A}^1_{bdb} & \mathbf{0} \\ \bar{\mathbf{B}}^{2^{-1}}_{bb}\mathbf{A}^2_{bdc} & \mathbf{0} & \bar{\mathbf{B}}^{2^{-1}}_{bb}\mathbf{A}^2_{bdb} \end{bmatrix} = \begin{bmatrix} \mathbf{K}^1_{cc} + \mathbf{K}^2_{cc} & \mathbf{K}^1_{cb} & \mathbf{K}^2_{cb} \\ \mathbf{K}^1_{bc} & \mathbf{K}^1_{bb} & \mathbf{0} \\ \mathbf{K}^2_{bc} & \mathbf{0} & \mathbf{K}^2_{bb} \end{bmatrix} \\ \mathbf{V}_{as} \equiv \mathbf{V}_{sss} = \begin{bmatrix} \bar{\mathbf{B}}^{-1}_{cc}\bar{\mathbf{A}}_{cvc} & \bar{\mathbf{B}}^{-1}_{cc}\bar{\mathbf{A}}^1_{cvb} & \bar{\mathbf{B}}^{-1}_{cc}\bar{\mathbf{A}}^2_{cvb} \\ \bar{\mathbf{B}}^{1^{-1}}_{bb}\mathbf{A}^1_{bvc} & \bar{\mathbf{B}}^{1^{-1}}_{bb}\mathbf{A}^1_{bvb} & \mathbf{0} \\ \bar{\mathbf{B}}^{2^{-1}}_{bb}\mathbf{A}^2_{bvc} & \mathbf{0} & \bar{\mathbf{B}}^{2^{-1}}_{bb}\mathbf{A}^2_{bvb} \end{bmatrix} = \begin{bmatrix} \mathbf{V}^1_{cc} + \mathbf{V}^2_{cc} & \mathbf{V}^1_{cb} & \mathbf{V}^2_{cb} \\ \mathbf{V}^1_{bc} & \mathbf{V}^1_{bb} & \mathbf{0} \\ \mathbf{V}^2_{bc} & \mathbf{0} & \mathbf{V}^2_{bb} \end{bmatrix} \end{cases} \tag{1.19}$$

It is now obvious that both methods produce exactly the same systems.

1.3 Analytical Models

The two analytical FE models that were used were created in FEMAP and solved with MD Nastran. NX Nastran was used for verification where non-reduced models were solved.

1.3.1 Blade

A version of the blade FE model described in [20] (Nastran model can be found online at [12]) was used and is visualised in Fig. 1.1. The model consisted of 20,523 nodes and 96,416 elements. The model has a solid core, for which solid elements were used and a laminate skin model, for which laminate plate elements were used. For a thorough explanation of the composite material model and how it was calibrated, see Johansson et al. [20] (Fig. 1.2).

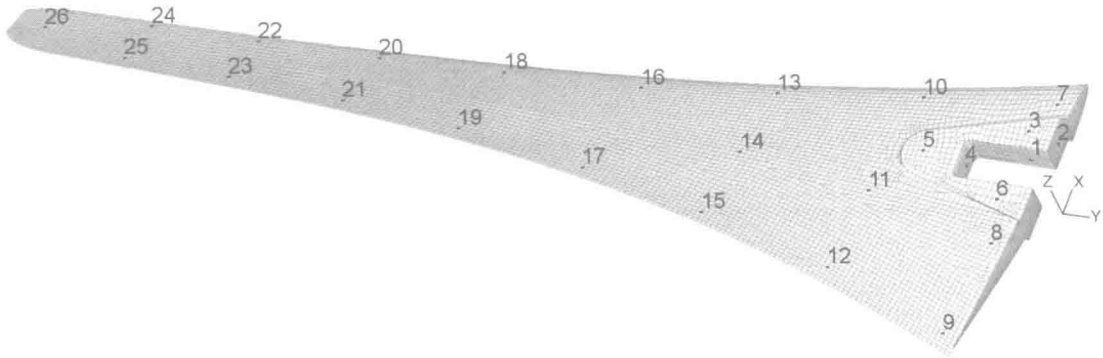

Fig. 1.1 FE model of the blade with numbering used in the FE model but also during the vibration tests

Fig. 1.2 Close-up view of the three inputs of the blade

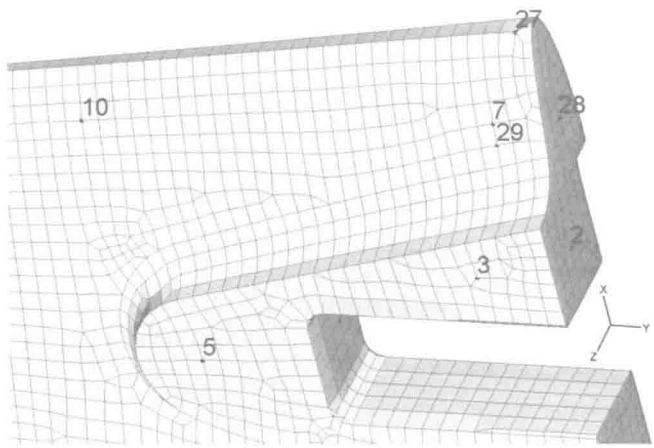

The accelerometer positions in the vibrations test and for the FE blade model are shown in Fig. 1.1. These were chosen as close to the physical locations of the accelerometers as possible for the MAC correlations to yield correct results. Note that the numbering starts at the coupling positions.

1.3.2 Bracket

The bracket geometry was received from TU Delft. It was modelled by 24,707 solid parabolic elements and an isotropic material model with stiffness $E = 2 \cdot 10^{11}\,\mathrm{N/m^2}$ and density $\rho = 5{,}000\,\mathrm{kg/m^3}$. The shaft which is inserted into the bracket was modelled as an integrated part of the bracket. Parabolic elements were used so that the shaft curvature would be described better. The bracket model is shown in Fig. 1.3. The numbers 1, 2 and 3 are the coupling positions coupled to the blade at positions 3, 4 and 5, thus matching DOFs were used at each of the components coupling locations.

1.3.3 FE Coupling

The coupling between the blade and the bracket can be seen in Fig. 1.4a, b, where the area around the holes on the blade have been constrained with rigid links. All the DOFs on the bracket in contact with the blade when mounted were constrained with rigid links to a six DOFs node located at the centre of the three holes. The bracket coupling type was constrained at the holes, see Fig. 1.4b. The same configurations were used in the experimental-analytical coupling. All three configurations were used in coupling of the analytical models. It should be noted that the blade bracket constraints configuration are on the same side of the blade which creates asymmetric modeshapes.

The assembled blade bracket structure along with the measurement points can be seen in Fig. 1.5.

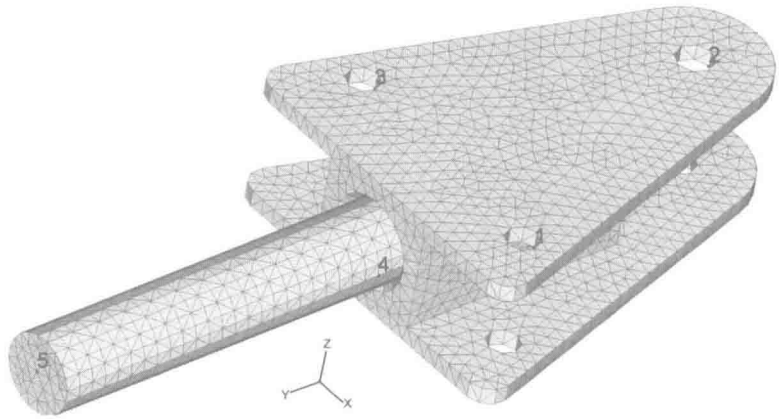

Fig. 1.3 FE model of the blade with numbering used in the FE model and during the vibration tests

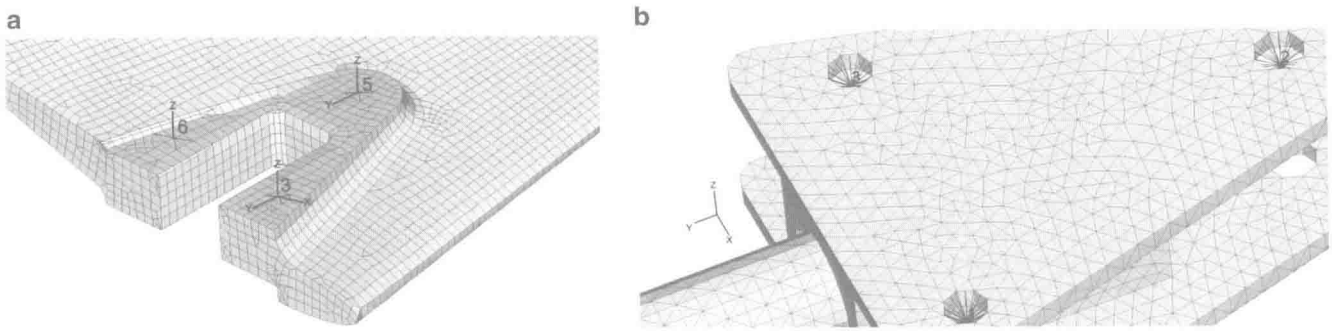

Fig. 1.4 The coupling configurations for the blade and the bracket using rigid links attached to a six DOFs coupling node. (**a**) Blade coupling configuration. (**b**) Bracket coupling configuration

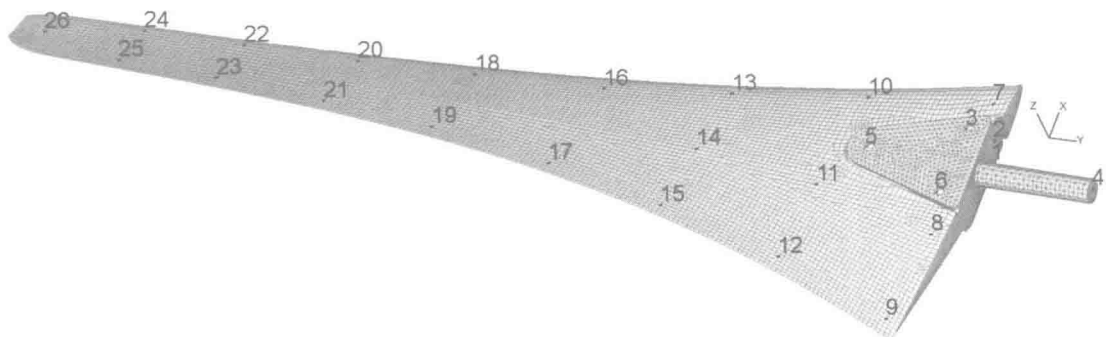

Fig. 1.5 The FE model of the blade mounted to the FE model of the bracket with measurement locations

1.4 Experiments

Three different blades from the same Ampair 600 wind turbine were considered. Each blade had a unique mounting brackets so that each blade was mounted to its own bracket. The three experimental blades will henceforth be denoted by their serial number; 841, 722 and 819 and the brackets will be numbered, 01, 02 and 03. Coupling between the blade and their corresponding bracket was blade 841 and bracket 01, blade 722 and bracket 02 and blade 819 and bracket 03. The bracket numbers will usually be omitted when the blade bracket configuration is discussed but occasionally they will be abbreviated as blade/bracket, e.g. 841/01 would represent a blade 841 which in turn is mounted to bracket 01.

The experiments were performed at Chalmers Vibration and Smart Structures Lab. The measurements were performed with a stepped sine input with 0.25 Hz step size from 20 to 800 Hz for the blade and blade bracket measurements. For the fully assembled system the measurements were performed from 10 to 300 Hz with a step size of 0.1 and 0.01 Hz at some particular frequency intervals. A total of three measurements for the blade and blade bracket models were made. The configurations

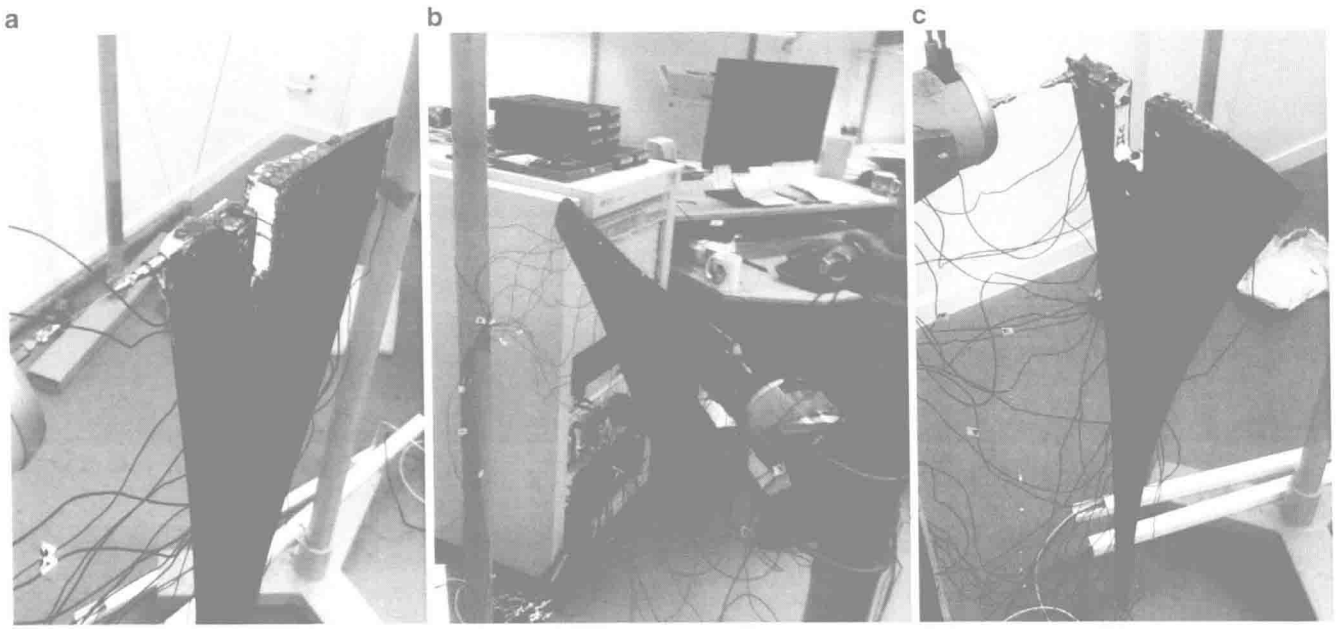

Fig. 1.6 The input directions and test setup for the blades. (**a**) Input in the x direction. (**b**) Input in the y direction. (**c**) Input in the z direction

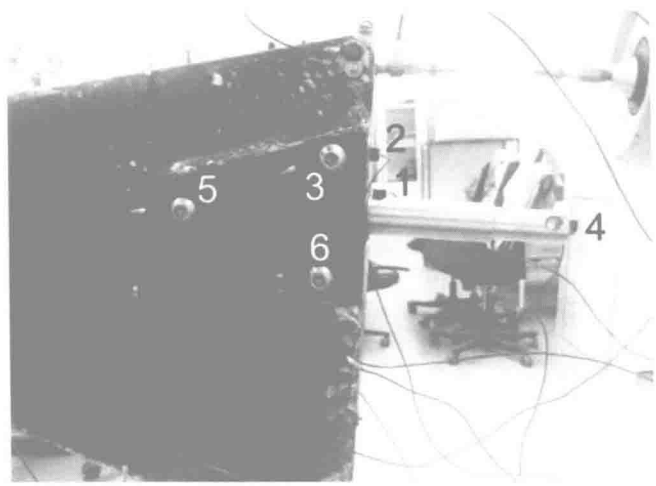

Fig. 1.7 A detailed view of the blade bracket assembly is shown with the accelerometer placements

considered were: the three blades alone and the three blades with brackets mounted. Note that measurements made in a specific direction (x, y or z) means that the input was aligned with that axis. See Fig. 1.1 for an orientation of an generic blade and Fig. 1.2 for the different input locations.

1.4.1 Test Setup

The three different input directions are shown in Fig. 1.6. This coordinate system is consistent with the FE analysis coordinate system. The test setup shown in Fig. 1.4 is also general for all measurements. It was exactly the same, both for the measurement of blades alone and for the blade measurements with a bracket attached. It can be seen, from Fig. 1.6, that the measured blades (and bracket mounted blades) were hung at three locations when measured in the x and y directions, which made it easier to position the components relative to the load cell. Measurements in the z direction for the blade and blade with attached bracket were only hung at two positions. Further, it should be noted that the components were hung in fasteners which were glued to the components, the same fastener was used for the load cell attachment and can be seen in Fig. 1.7. All the fasteners were mounted on the blades during all measurements for consistency.

The interface locations of the blade are shown in Fig. 1.2 but with the interface accelerometer from position 6 located under the stinger and used as a direct accelerance for a comparison with the accelerometer at position 1.

For a view of a bracket and blade assembled see Fig. 1.7. A detailed view of the interface accelerometers can also be seen. Different input directions to the bracket coupled with a blade had the same accelerometer locations and the same input locations were used as shown in Fig. 1.6.

1.5 Experimental Models

To obtain experimental models, system identification was performed on the obtained frequency response data (FRD). The system identification of the substructures, see Sect. 1.4.1, was conducted using an automated method for order selection and identification developed by Yaghoubi and Abrahamsson, see [29, 32]. This method is based on obtaining a number of realisations of the same dataset, using MATLAB's `n4sid` method, which is a state-space subspace method, see McKelvey et al. [28]. The realisations is then statistically evaluated, using the MOC, to discard non-physical modes. The only input required by the user is a high model order from start. In general, the method worked very well for the experimental data of the blade. Only occasionally did it give non-physical modes that could be removed manually. The synthesised models correlate well with measured data and the spread in response between the different blades can be seen in Fig. 1.8.

1.6 Results

In this section correlation between the eigenvalues of the blade models and the blade bracket coupled models are presented. Then, analytical coupling between the components is presented together with the experimental-analytical coupling results. Comparisons between the state-space and the frequency-based methods compared to analytical coupling and finally results based on measurements compared to experimental-analytical coupling.

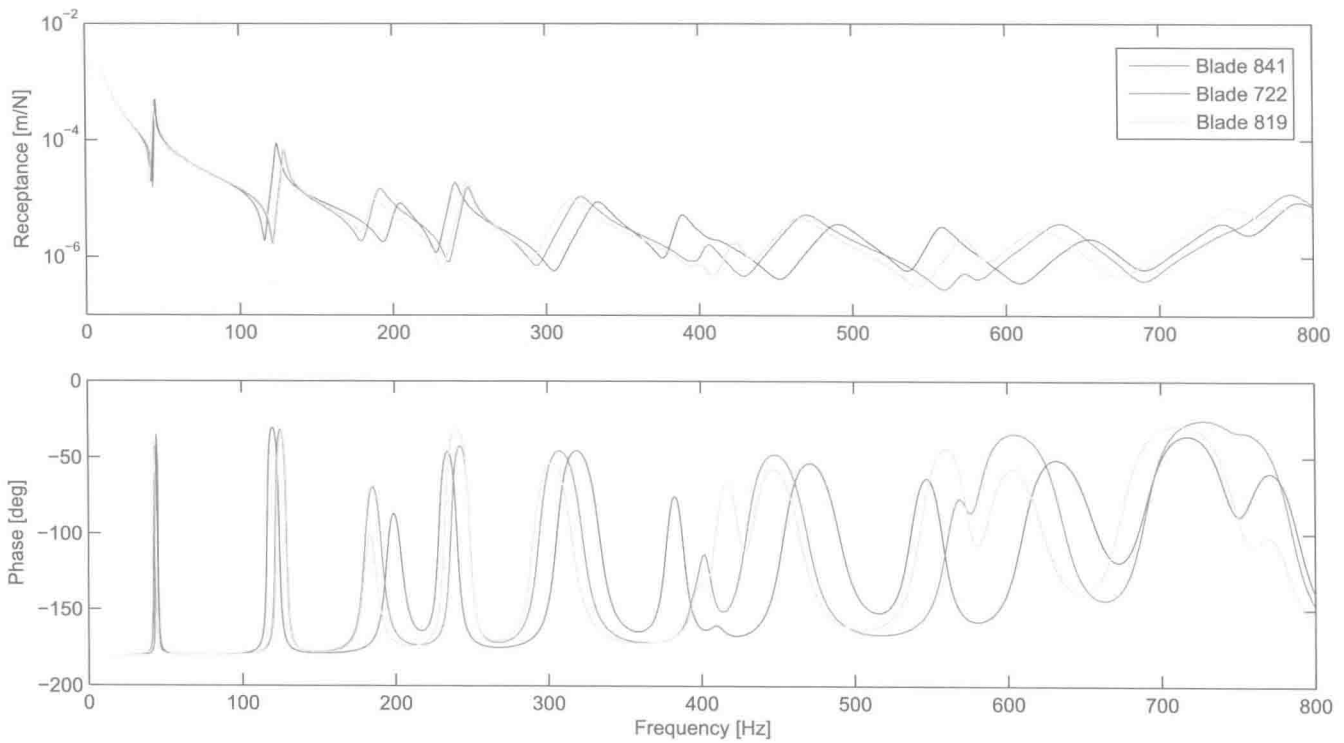

Fig. 1.8 Spread between the synthesised FRFs of the blades with input in z and output from channel 7